



Published in final edited form as:

Biomacromolecules. 2010 December 13; 11(12): 3219–3227. doi:10.1021/bm100469w.

A Complete Recombinant Silk-Elastinlike Protein-Based Tissue Scaffold

Weiguo Qiu[†], Yiding Huang[†], Weibing Teng[†], Celine M. Cohn[§], Joseph Cappello[‡], and Xiaoyi Wu^{*,†,§}

Department of Aerospace and Mechanical Engineering, Biomedical Engineering IDP and Bio5 Institute, University of Arizona, Tucson, Arizona 85721, USA, and Protein Polymer Technologies, Inc., San Diego, California 92121, USA

Abstract

Due to their improved biocompatibility and specificity over synthetic materials, protein-based biomaterials, either derived from natural sources or genetically engineered, have been widely fabricated into nanofibrous scaffolds for tissue engineering applications. However, their inferior mechanical properties often require the reinforcement of protein-based tissue scaffolds using synthetic polymers. In this study, we report the electrospinning of a completely recombinant silk-elastinlike protein-based tissue scaffold with excellent mechanical properties and biocompatibility. In particular, SELP-47K containing tandemly repeated polypeptide sequences derived from native silk and elastin was electrospun into nanofibrous scaffolds, and stabilized via chemical vapor treatment and mechanical preconditioning. When fully hydrated in 1x PBS at 37 °C, mechanically preconditioned SELP-47K scaffolds displayed elastic moduli of 3.4 to 13.2 MPa, ultimate tensile strengths of 5.7 to 13.5 MPa, deformabilities of 100 to 130% strain, and resilience of 80.6 to 86.9%, closely matching or exceeding those of protein-synthetic blend polymeric scaffolds. Additionally, SELP-47K nanofibrous scaffolds promoted cell attachment and growth demonstrating their *in vitro* biocompatibility.

Introduction

Protein-based biomaterials are appealing for tissue engineering applications because of their improved biocompatibility and specificity.¹ For instance, natural proteins such as collagen and elastin have been fabricated into nanofibrous scaffolds.^{2,3} However, their properties are often limited by the inherent properties of the natural protein or the harsh chemical methods used in their preparation. The advent of recombinant protein engineering has enabled the preparation of new protein-based biomaterials containing precisely controlled polypeptide sequences.^{1,4,5} As such, recombinant proteins can be designed to mimic certain physical and biological properties of their parent protein as well as provide novel properties or novel combination of properties useful, for example, in the manufacture or fabrication of the material. As an example, recombinant elastinlike proteins display elasticity and other physical properties characteristic of native elastin^{6–11}, and silklike proteins form β -sheet crystals that are responsible for the high tensile strength of native silks^{12–14}. Combined in

*To whom correspondence should be addressed. Tel.: 1-00-520-626-5854. Fax: 1-00-520-621-8198. xwu@email.arizona.edu.

[†]Department of Aerospace and Mechanical Engineering.

[‡]Protein Polymer Technologies.

[§]Biomedical Engineering IDP and Bio5 Institute.

Supporting Information Available. Optical images of sample thickness measurement. A representative force-clamp gap curve. Preconditioning displacement and force measurement. This information is available free of charge via the Internet at <http://pubs.acs.org>.

the same protein chain, multi-block protein copolymers in which individual blocks confer distinct mechanical, chemical or biological properties can provide useful properties not obtainable from the parent proteins alone.^{15–17} In particular, we have produced a series of silk-elastinlike proteins (SELPs) consisting of polypeptide sequences derived from silk for superior mechanical strength and from elastin for durability and resiliency.^{16,18} Notably, the silklike blocks are capable of crystallizing to form physical cross-links between elastin-mimetic sequences, which, in turn, decrease the crystallinity of the polymer and thus enhance the solubility of the SELPs. Consequently, SELPs may be fabricated into a variety of useful structures for biomedical applications.^{18–21}

Despite their enhanced biocompatibility and cellular functions, protein-based materials generally possess inferior mechanical properties over synthetic polymers. As a result, they are often blended with synthetic polymers to produce tissue scaffolds with improved biocompatibility while retaining sufficient mechanical strength.^{22,23} However, the biodegradation products of synthetic polymers may pose biocompatibility and toxicity risks, thereby compromising the long-term performance of tissue scaffolds. For example, when polyglycolic acid (PGA) scaffolds are used to grow a human artery, undifferentiated phenotypes of smooth muscle cells are observed in proximity to residual PGA fragments.²⁴ In contrast, the biodegradation products of protein-based materials, which are peptides composed of natural amino acids, may avoid these risks. Therefore, the development of a completely protein-based scaffold with appropriate mechanical properties is vigorously sought in tissue engineering.

In this study, we explore the potential of SELPs in the engineering of a completely protein-based, mechanically robust tissue scaffold. The design of SELPs is to impart the high tensile strength of silk and the excellent resilience of elastin into a single protein. Indeed, SELPs in the form of thin films and micro-diameter fibers displayed high tensile strength and deformability and excellent resilience.^{21,32} In addition to polypeptide sequence, a number of processing parameters may influence the structure and property of silk-based materials. For instance, underwater spinning³³ and fast reeling studies³⁴ of silk suggest that shear and elongation stresses enhance the molecular orientations and thus the mechanical properties of silk fibers. It is believed that an extended extrusion of silk leads to enhanced molecular orientations and increased mechanical strength and fracture toughness. We thus hypothesize that SELP nanofibrous scaffolds may possess improved mechanical properties if compared to SELP thin films and micro-diameter fibers.

Here, SELP was fabricated into nanofibrous scaffolds using the electrospinning technique. Among many fabrication techniques, electrospinning has emerged as a versatile method for fiber formation.²⁷ As a result, numerous nanofibrous tissue scaffolds have been electrospun from synthetic polymers^{28,29} as well as proteins^{3,30}. Recently, nanofibrous scaffolds electrospun from type I collagen displayed good tensile strength.³¹ In the electrospinning of SELPs, extended stretching of protein polymer molecules and enhanced molecular orientations can be achieved through electrostatic forces, leading to improved mechanical properties. The resulting SELP scaffolds were further stabilized via different chemical vapor treatments (i.e., methanol, glutaraldehyde, combined methanol and glutaraldehyde). The silklike sequence of SELPs is capable of crystallizing to provide the SELP structures mechanical strength. Treatment using methanol or other non-solvents can accelerate this crystallizing process. Additionally, lysine residues present in SELP-47K permit chemical crosslinking of the elastinlike blocks using glutaraldehyde. Changes in the secondary structures of the SELP scaffolds due to the crystallization of the silklike blocks and the crosslinking of the elastinlike blocks were examined using Fourier transform infrared (FTIR) spectroscopy. The mechanical properties of the SELP scaffolds, including tensile strength, elastic modulus, deformability, and resilience, were evaluated. The cell

compatibility of the scaffolds was also assessed using *in vitro* cell viability and proliferation assays.

Materials and Methods

Scaffold Fabrication

Frozen SELP-47K (884 amino acid chain length; MW 69,814) aqueous solution at a concentration of 13 w/w% was generously provided by Protein Polymer Technologies, Inc. (San Diego, CA). The protein polymer has a monomer structure of (E)₄(S)₄(EK)(E)₃, in which S is the silklike sequence GAGAGS, E is the elastinlike sequence GVGVP, and EK is the pentapeptide sequence GKGVP. The complete amino acid sequence of SELP-47K was previously reported,¹⁸ while its purity and molecular weight were examined by MALDI-TOF and SDS-PAGE.³² The SELP-47K solution was lyophilized and redissolved in 98% formic acid (VWR) at various concentrations (i.e., 250, 200, 150, 75, 50 mg/mL) for fiber electrospinning.

A custom-built electrospinning device, comprised of a Gama High Voltage DC power and a syringe pump (Braintree Scientific, MA), was used for the fabrication of SELP-47K nanofibers. Briefly, protein solutions of SELP-47K copolymer formed a droplet at the orifice of a 32 gauge stainless steel needle. The droplet was then stretched and splayed into a series of fine filaments under a high-voltage electric field. The generated SELP-47K nanofibers were collected on aluminum foil, silicon die, or glass slides, which were placed on a grounded steel plate as a secondary collector. A voltage of 20 KV was applied, the distance between the needle tip and collector was fixed at 12 cm, the solution feed rate was 0.1 ml per hour, and the temperature and relative humidity were 23 ± 2 °C and $24 \pm 2\%$, respectively. Scaffolds of about 10 μ m were obtained from the electrospinning of SELP-47K solution for 9 hours.

Scaffold Treatment

Electrospun SELP-47K nanofibrous scaffolds were treated for 48 hrs with methanol (MeOH), glutaraldehyde (GTA) or combined MeOH and GTA vapor (48 hrs with MeOH and 48 hrs with GTA) in a vacuumed dessicator. A petri dish containing 10 ml of 25% GTA^{35,36} or 99.9% MeOH was placed at the bottom of the dessicator. SELP-47K scaffolds collected on aluminum foil or glass slides were placed on a ceramic plate with holes, which separated the bottom chamber with chemicals from the top chamber. Treated SELP-47K nanofibrous scaffolds were then peeled off the aluminum foil for Scanning Electron Microscopy (SEM), FTIR and mechanical analysis, or kept on the glass slides for further treatment and cellular studies.

Scaffold Characterization

Four types of SELP-47K scaffolds, including as-spun, MeOH-, GTA-, and MeOH-GTA-treated scaffolds, were analyzed using SEM and FTIR. The surface morphologies of vacuum-dried, platinum-coated SELP-47K scaffolds after different treatments were examined using a Hitachi-S4800 field emission scanning electron microscope (FESEM). To investigate fiber bifurcation, SELP-47K nanofibers were collected for SEM analysis on 1.2 cm \times 1.2 cm silicon wafers at a very low fiber density by limiting the fiber collection time.

A Magna-IR 560 Nicolet spectrometer (Madison, WI) equipped with a CsI beam splitter and DTGS-detector was used to analyze the secondary structures of SELP-47K nanofibrous scaffolds. The spectrometer was purged continuously with dry air. FTIR spectra over the range of 4000-800 cm^{-1} were acquired using 400 scans of both sample and reference at a 4

cm⁻¹ resolution. The FTIR data were collected on three replicate samples. Data collection was performed using Omnic processing software provided by Nicolet.

Mechanical Analysis

Uniaxial tensile analysis of hydrated SELP-47K scaffolds was performed on a PerkinElmer dynamic mechanical analyzer (DMA). SELP-47K nanofibrous scaffolds were first cut into rectangular strips, the thickness of which were measured using an optical microscope. As shown in Fig. S1, a hydrated sample was wrapped around a metal pin and taped. The metal pin with the sample was immersed in 1x PBS and imaged, and the sample thickness was calculated from the optical images. Samples were mounted onto the DMA with a gap of 3 mm between the clamps, which was further reduced to 1.5 mm to prevent any stress buildup induced by the shrinkage of samples upon soaking. Samples were immersed in a jacketed beaker filled with 1x PBS at 37 °C, equilibrated for 1 hr before test, and evaluated by each of two mechanical test protocols. (1) Monotonic stress-strain. Samples were stretched to break, and the Young's modulus, ultimate tensile strength, and strain at failure of SELP-47K scaffolds were obtained. Due to imperfect sample loading, a sample may be slightly buckled and its gauge length may not be exactly 3 mm. The true gauge length of samples, which was close to 3 mm, was determined from the force-extension curve, as illustrated in Fig. S2. (2) Mechanical preconditioning. Samples of about 3 mm in length were cyclically stretched for 6 cycles between 1.5 mm and 4.0 mm (Fig. S3A), and then stretched to break. This will lead to preconditioning strain of about 33% (displacement of 1 mm over the original sample length of 3 mm) and an off-loading period of 5 min between cycles. Resilience was calculated from the loading and unloading curves as follows.

$$\% \text{resilience} = 100 * \text{area under unloading curve} / \text{area loading curve}$$

Reproducibility was examined using seven replicate samples for each type of SELP-47K nanofibrous scaffolds, including MeOH-, GTA-, and MeOH- and GTA-treated scaffolds. Throughout this study, loading and unloading were controlled by displacement at a fixed rate of 250 μm/min.

Cell Culture

After post-fabrication treatment, SELP-47K nanofibrous scaffolds along with a glass slide were sterilized by immersion in 70% ethanol overnight, incubated in culture medium for 4 hrs to promote cell attachment, peeled off from the glass slide, and punched into circular disks of 8 mm in diameter. The circular scaffold samples were rinsed three times with cell culture grade 1X PBS, transferred to a 48-well cell culture plate, seeded with 10 μL of NIH/3T3 fibroblast suspension at a density of 300 cells/μL, and incubated in an incubator at 37°C with 5% CO₂ for 7 days or until cells reached 100% confluence. As a control study, cells were also cultured in a tissue culture polystyrene (TCPS) well without SELP-47K nanofibrous scaffolds.

Scaffold samples 6 days after cell culture were prepared for SEM analysis. Briefly, samples were soaked in a primary fixation solution (4% formaldehyde, 1% GTA in 0.1 M phosphate buffer), fixed by 1% osmium tetroxide, rinsed with buffer, dehydrated through a series of graded alcohol solutions and then dried with a Polaron critical point drier using liquid carbon dioxide. The specimens were coated with platinum and viewed by a Hitachi-S4800 SEM.

Cell Viability

Cell viability was examined 5 days after cell culture using the LIVE/DEAD Viability/Cytotoxicity Kit (Invitrogen), according to the manufacturer's instructions. After removing culture medium, samples were rinsed three times with cell culture-grade 1X PBS and then incubated for 30 minutes with 120 μ l of staining solution containing 2 IM calcein AM and 4 IM EthD-1. Live and dead cells were imaged under a fluorescent microscope (Leica DMI 4000 B) after removing the staining solution and rinsing cells once with 1X PBS.

Cell Proliferation

Cell proliferation was analyzed by the MTS assay (CellTiter 96 AQueous Assay, Promega) on days 1, 3, 5, and 7. Live cells react with a tetrazolium salt in the MTS reagent producing a soluble formazan dye, which has absorbance at a wavelength of 490 nm. Within the linear region of the absorbance curve, cell number is proportional to the absorbance intensity, measured using a Nanodrop UV-Vis spectrophotometer (Thermo Scientific).

Statistical Analysis

Cell attachment, viability and proliferation were analyzed on multiple replicates, and measurements were expressed as mean \pm standard deviation (SD). The student's t-test analysis of variance (SigmaPlot) was employed to assess statistical significance of the results. Difference was considered statistically significant when $p < 0.05$.

Results and Discussion

Scaffold Fabrication

Many factors may influence the micro-architecture of an electrospun scaffold, such as its fiber diameter, surface morphology, and pore size. Adjustments of factors such as voltage, the distance between the spinneret and collector, and feed rates were made in order to establish conditions yielding good quality nanofibers (data not shown). One factor, the influence of SELP solution concentration on fiber micro-architecture was of particular interest. At low concentrations (e.g., 5% w/v), evident was the formation of SELP-47K filament of 10 to 30 nm in diameter and submicron droplets (Fig. 1A). Interestingly, charge accumulation on a micro-droplet drastically altered the local deposition of SELP-47K nanofilaments. More concentrated SELP-47K solutions would enhance polymer chain entanglement and thus solution elasticity. Consistent with a study by Yu et al.³⁸, the enhanced elasticity of concentrated SELP-47K solutions (e.g., 150 and 200 mg/mL) suppressed the Rayleigh instability and arrested the break-up of the jet into droplets, leading to the formation of bead-free nanofibers (Fig. 1B). However, if the viscosity of SELP-47K solution (e.g., 250 mg/mL) is too high, some jets of SELP-47K solutions may not be fully stretched by the electrostatic force, leading to the generation of beads-on-a-string structures (Fig. 1C). The formation of SELP-47K nanofibers suggests that formic acid was removed during the electrospinning process and the jet of SELP-47K solutions was solidified before reaching the collector. Nevertheless, SELP-47K nanofibers electrospun from a 150 or 200 mg/mL solution have non-uniform diameters (Fig. 1D). While the majority of fibers were 50 to 200 nm in diameter, some larger fibers of a few hundred nanometers in diameter were also observed (Figs. 1B, 1D).

Nanofibers electrospun from a 150 mg/mL solution were examined at both sides of the SELP-47K scaffolds. At the side closer to the glass slide, two populations of nanofibers were observed: small fibers of 10 to 30 nm in diameter and large fibers of 100 to 300 nm in size (Fig. 2A). On the side closer to the needle, only fibers of 100 to 300 nm in diameter were observed (Fig. 2B). Likely, small fibers of 10 to 30 nm in size were first formed and deposited on the collector, leading to the build-up of charges on the collector surface. The

charge build-up may alter the local electrostatic field, affecting the subsequent fiber formation and branching.

SEM analysis of SELP-47K nanofibers collected on silicon dies at a low fiber density revealed fiber branching or bifurcation (Fig. 3). In particular, thin lateral fibers were branched from the primary fibers, appearing to be more prone to bending instability during the electrospinning process. Yarin et al. proposed that for spinnable polymer solutions, the combination of the electric Maxwell stress and surface tension may induce undulation of the solution jet, the instability of which can lead to the emanation of lateral branches.³⁹ This mechanism may explain the branching of SELP-47K nanofibers. Moreover, a laterally branched fiber observed in the electrospinning of SELP-47K nanofibers showed a gradually decreased diameter, and eventually terminated. Although the underlying mechanism behind this phenomena is not fully understood, fiber branching is likely responsible for the non-uniform diameter distribution of electrospun SELP-47K nanofibers. While large fibers may possess enhanced mechanical properties, small fibers of large surface areas can promote cell adhesion and growth. Therefore, non-uniformity of SELP-47K nanofibers will not compromise their applications in tissue engineering. Recently, hybrid electrospinning was designed to fabricate poly(D,L-lactide-co-glycolide) (PLGA) scaffolds containing both large and small fibers, in order to improve mechanical and cellular properties.⁴⁰

Post-fabrication Treatment

Unlike many synthetic polymer fibers, electrospun protein fibers often need to be chemically crosslinked to attain sufficient mechanical strength and stability to be used under physiologically relevant conditions.^{41,42} In our previous work we demonstrated that SELP-47K could be chemically crosslinked by either covalent or non-covalent means. In each monomer of SELP-47K (i.e., (E)₄(S)₄(EK)(E)₃), a lysine residue replaces one of the valine residues in the 8 repeats of the elastinlike pentapeptide sequence. Glutaraldehyde can react with lysine residues to covalently crosslink SELP-47K. Likewise, we have shown that methanol can induce the crystallization of the silklike blocks, essentially forming non-covalent crosslinks in SELP-47K. Electrospun fibrous scaffolds of SELP-47K were treated with MeOH, GTA or a combination of MeOH and GTA vapor, resulting in excellent inter-fiber bonding and the formation of an integrated, porous, fibrous scaffold (Fig. 4). Pore size was 1.40 ± 0.87 , 1.37 ± 0.83 , 1.05 ± 0.60 , and 1.09 ± 0.54 μm for as-spun, MeOH-, GTA-, and MeOH-GTA-treated scaffolds, respectively. While MeOH-treatment alone induced little changes in pore size, GTA- and MeOH-GTA treatment reduced pore size up to 25%.

Secondary Structure

Methanol and glutaraldehyde treatments may induce the crystallization of the silklike blocks and the crosslinking of the elastinlike blocks, leading to changes in the secondary structure of SELP-47K fibrous scaffolds. Such secondary structural changes were examined using FTIR (Figs. 5A, 5B). Non-treated SELP-47K scaffolds displayed a broad band at 1660 cm^{-1} , indicating the dominance of β -turn and unordered conformations.⁴³ Upon MeOH or GTA treatment, the amide I band of SELP-47K scaffolds split into two: one at 1653 cm^{-1} that is the characteristic of unordered structure and the other at $1628\text{--}1635 \text{ cm}^{-1}$ typical of antiparallel β -sheets. The emerged band at $1628/35 \text{ cm}^{-1}$ suggested that post-fabrication treatment resulted in a partial transition from Silk I structure dominated by unordered conformations to Silk II structure characterized by β -sheet conformation. This was confirmed by the appearance of a shoulder at 1700 cm^{-1} , and consistent with the shifting of the amide A band to a lower wavenumber (from 3310 cm^{-1} to 3290 cm^{-1}), indicating more involvement of NH bonds in hydrogen bonding. Nevertheless, the double amide I bands and their breadth revealed the coexistence of other conformations. Indeed, Silk I markers at 1410 cm^{-1} ($\text{C}_\alpha\text{H}_2$ stretching⁴⁴), 1330 cm^{-1} (CH_3 symmetric stretching), and 1387 cm^{-1} (CH_3

stretching⁴⁵), identified by Taddei and Monti⁴³, were all displayed by MeOH-, GTA-, and MeOH-GTA-treated SELP-47K nanofibrous scaffolds (Fig. 5A). The partial Silk I to Silk II conversion is associated with the enhanced stability of treated SELP-47K scaffolds.

Mechanical Analysis

Mechanical properties of SELP-47K nanofibrous scaffolds were analyzed when samples were fully hydrated in 1x PBS at 37 °C. The width and length of hydrated MeOH-, GTA-, MeOH-GTA-treated samples were 94 ± 2 , 102 ± 1 and $108 \pm 2\%$ of their dry counterparts, respectively. However, their thicknesses were 143 ± 8 , 68 ± 4 and $70 \pm 4\%$ of their dry counterparts, respectively. In this study, stress calculation is based on the dimensions of hydrated samples. Uniaxial tensile analysis of MeOH-treated scaffolds revealed an ultimate tensile strength of 7.2 ± 2.3 MPa, and strain at failure of $130 \pm 30\%$, and Young's modulus of 3.7 ± 1.2 MPa that was measured in the first 20% strain region (Fig. 6, Table 1). GTA-treated SELP-47K scaffolds displayed a Young's modulus of 18.2 ± 3.3 MPa, ultimate tensile strength of 14.1 ± 3.8 MPa, and strain at failure of $130 \pm 40\%$. Likewise, MeOH-GTA-treated scaffolds possessed mechanical properties comparable to scaffolds treated by GTA alone. Compared to the bulk mechanical properties of SELP-47K films under the same chemical treatments,³² the Young's modulus and tensile strength of SELP-47K nanofibrous scaffolds were 3 to 5 fold greater, while their deformability was comparable. Among others⁴⁶, we previously reported that wet-spun microfibers of smaller diameter possessed higher Young's modulus and tensile strength.²¹ It is believed that an increased molecular orientation in smaller fibers and mechanical properties can be obtained using smaller spinnerets and/or through larger post-fabrication stretching.

Mechanical preconditioning is often used to stabilize the microstructure of soft tissue materials, permitting the measurement of repeatable mechanical properties.⁴⁷ The influence of mechanical preconditioning on the material behavior of electrospun SELP-47K nanofibrous scaffolds was examined by subjecting hydrated samples to 6 repetitive cyclic strains of about 34% (Fig. 7). Although mechanical preconditioning had little influence on the mechanical behavior of SELP-47K scaffolds after the preconditioning strains, it greatly influenced the material response to cyclic deformations within the preconditioning strain. The resilience of a scaffold, which characterizes its capacity for shape and energy recovery under mechanical loading, was evaluated using formula (1). Without preconditioning, GTA-, MeOH-, and MeOH-GTA-treated scaffolds possessed resilience of $45.9 \pm 3.6\%$, $60.4 \pm 4.4\%$, and $59.5 \pm 6.7\%$, respectively (Fig. 8). The enhanced resilience of MeOH- and MeOH-GTA-treated scaffolds over that of the GTA-treated scaffold suggests that the crystallization of the silklike blocks induced by methanol treatment is more effective in limiting the chain rearrangement and thus reducing the hysteresis of electrospun scaffolds than is GTA treatment. Over the six loading cycles, a slight drop in peak stress was observed (Fig. 7), but the resilience of GTA-, MeOH-, and MeOH-GTA-treated scaffolds increased to $83.8 \pm 6.5\%$, $86.9 \pm 2.8\%$, and $80.6 \pm 5.4\%$, respectively (Fig. 8, Table 1). The greatest increase in resilience largely occurred after the first cycle, presumably due to stabilization of deformation-induced changes in scaffold microstructure. Significantly, the resilience of the SELP-47K scaffolds after preconditioning (80~87%) approached that of native elastin, which is 90%.^{48,49}

Table 2 compares the mechanical properties of SELP-47K nanofibrous scaffolds with those of other protein-based nanofibrous scaffolds. While nanofibrous scaffolds have been electrospun from other proteins,⁵⁹ few have been mechanically analyzed in physiologically relevant conditions.^{31,51,52} We²¹ and others⁶⁰ have noted, the mechanical properties of protein-based materials change dramatically between the dry state and the fully hydrated state. Moreover, the mechanical behavior of fully hydrated scaffolds is more relevant to applications in tissue engineering.

As shown in Table 2, SELP-47K scaffolds possess ultimate tensile strengths comparable to those of GTA-crosslinked type I collagen scaffolds³¹ and far exceed those of fibrinogen scaffolds⁵⁰. The ultimate tensile strengths of MeOH- and MeOH-GTA-treated SELP-47K scaffolds closely match or even exceed those of collagen-blended PDO and silk-blended PEO scaffolds,^{51,53} but are inferior to those of PLGA-reinforced gelatin/elastin scaffolds.⁵² In contrast, SELP-47K scaffolds possess elastic modulus (3.4~13.2 MPa) that are significantly higher than those of native elastin (0.1~1.1 MPa),⁵⁴⁻⁵⁶ although their deformability is comparable to that of native elastin. Additionally, the elastic moduli of SELP-47K nanofibrous scaffolds are comparable to those of human coronary and femoral arteries,^{51,58} yet lower than that of human saphenous vein.⁵¹ In terms of ultimate tensile strength, they are stronger than human coronary/femoral arteries and saphenous vein.^{51,57,58} Still, their deformability is similar to that of native arteries and polymer-reinforced collagen, gelatin/elastin and silk scaffolds.

To summarize, electrospun SELP-47K nanofibrous scaffolds display mechanical properties (e.g., elastic modulus, ultimate tensile strength, deformability) comparable to or exceeding those of native human arteries, collagen fibrils and electrospun collagen and fibrinogen scaffolds, possessing great potential for tissue engineering applications.

Cell Viability and Attachment

An ideal scaffold material should have excellent cyto-biocompatibility and promote cell attachment and growth. Revealed by a subcutaneous implantation study in rats, SELPs in the form of thin films displayed a protein sequence-dependent degradation/resorption and excellent *in vivo* biocompatibility.⁶¹ Recently, their use for gene therapy was also explored.⁶² In this study, the NIH/3T3 fibroblasts were used as a model system to evaluate the *in vitro* biocompatibility of SELP-47K nanofibrous scaffolds.

Cell viability was assessed using the LIVE/DEAD assay. After staining, live cells produce an intense green fluorescence while dead cells emit a bright red fluorescence. The cell viability assay revealed that most of the cells seeded on all the three types of SELP-47K nanofibrous scaffolds were alive (Fig. 9). Cell viability was quantified by counting the number of live cells versus the total cells in ten digital microfluorescence images of stained cells on each type of scaffold. The percent viability of 3T3 fibroblasts on MeOH-, GTA-, and MeOH-GTA treated scaffolds were determined to be $99.6 \pm 0.4\%$, $99.2 \pm 0.6\%$ and $93.5 \pm 2.5\%$, respectively. The high viabilities of 3T3 fibroblasts suggested that electrospun SELP-47K nanofibrous scaffolds are highly biocompatible.

SEM analysis revealed more detailed cell-material and cell-cell interactions on SELP-47K nanofibrous scaffolds. Images of individual 3T3 fibroblasts cultured on MeOH- and GTA-treated scaffolds for 6 days were presented in Fig. 10. Cells cultured on MeOH-GTA-treated scaffolds for 6 days completely covered the scaffolds (Fig. 12), preventing a direct analysis of cell-material interaction. As shown in Fig. 10A, many filopodia were formed on the surface of the cell, linking it to the SELP-47K scaffold (Fig. 10A). Interestingly, a cell lamellipodium managed to squeeze into a scaffold, interacting with finer SELP-47K nanofilaments (Fig. 10B). Cells interacted not only with SELP-47K nanofibrous scaffolds, but also with each other (Fig. 10C).

To evaluate the ability of SELP-47K nanofibrous scaffolds to support cell proliferation, 3T3 fibroblasts were seeded at the same density on all three types of scaffolds and in TCPS wells as a control. Their proliferation profiles were assessed using the MTS assay. During a period of 7 days, 3T3 fibroblasts cultured on SELP-47K scaffolds continuously grew in number, suggesting the ability of cells to proliferate on the scaffolds (Fig. 11). The proliferation of 3T3 fibroblasts slowed on day 7, as the cells approached 100% confluence on all three types

of scaffolds. While MeOH-treated SELP-47K scaffolds demonstrated cell proliferation slightly inferior to the culture control on TCPS, GTA- and MeOH-GTA-treated scaffolds displayed comparable or even better proliferation than the control. A close examination of SEM images suggests that more than one layer of cells were grown on MeOH-GTA-treated scaffolds (Fig. 12A). Cells were grown less confluent on GTA-treated scaffolds than those seeded on MeOH-GTA-treated scaffolds, permitting more detailed analyses of cell-cell interactions. A SEM analysis revealed the formation of ECM nanofilaments and filament sheets between cells (Fig. 12B). The regenerated ECM may provide additional surface areas for cell attachment and cell-cell interaction, leading to better cell proliferation. Together with the attachment and viability assays, the proliferation study shows that SELP-47K nanofibrous scaffolds display excellent cytocompatibility.

Conclusion

Recombinant silk-elastinlike protein polymer, SELP-47K, was electrospun into nanofibrous tissue scaffolds. FTIR spectroscopy suggested that chemical vapor treatment with MeOH, GTA, or MeOH-GTA partially induced a structural transition from Silk I to Silk II, resulting in the enhanced integrity and stability of the electrospun SELP-47K scaffolds. In contrast, the non-treated scaffolds are not stable in 1x PBS (data not shown). Indeed, mechanical analysis revealed that the elastic modulus, tensile strength, deformability and resilience of the SELP-47K scaffolds exceed those of collagen- and fibrinogen-based scaffolds and closely matched a number of protein-blended polymeric scaffolds. Additionally, optical and SEM microscopy demonstrated that 3T3 fibroblasts adhered to and spread on the scaffolds. Cells maintained excellent viability and proliferation rates on the SELP-47K scaffolds and in TCPS culture wells were similar. Future studies will evaluate these nanofibrous scaffolds for their potential applications in tissue engineering.

Supplementary Material

Refer to Web version on PubMed Central for supplementary material.

Acknowledgments

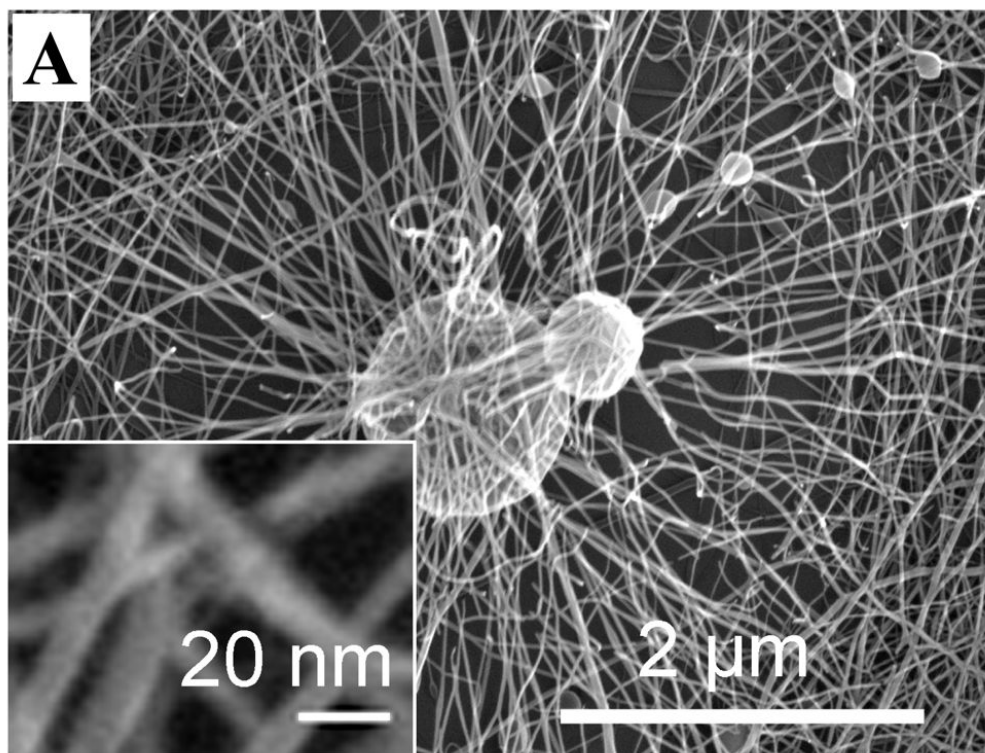
This research was supported by NIBIB (R21EB009160) and NSF (CMMI0856215).

References

1. Langer R, Tirrell DA. *Nature*. 2004; 428(6982):487–492. [PubMed: 15057821]
2. Li CM, Vepari C, Jin HJ, Kim HJ, Kaplan DL. *Biomaterials*. 2006; 27(16):3115–3124. [PubMed: 16458961]
3. Matthews JA, Wnek GE, Simpson DG, Bowlin GL. *Biomacromolecules*. 2002; 3(2):232–238. [PubMed: 11888306]
4. van Hest JCM, Tirrell DA. *Chemical Communications*. 2001; 19:1897–1904. [PubMed: 12240211]
5. Maskarinec SA, Tirrell DA. *Current Opinion in Biotechnology*. 2005; 16(4):422–426. [PubMed: 16006115]
6. Chilkoti A, Dreher MR, Meyer DE. *Advanced Drug Delivery Reviews*. 2002; 54(8):1093–1111. [PubMed: 12384309]
7. Lee TAT, Cooper A, Apkarian RP, Conticello VP. *Advanced Materials*. 2000; 12(15):1105–1110.
8. McMillan RA, Conticello VP. *Macromolecules*. 2000; 33(13):4809–4821.
9. Meyer DE, Chilkoti A. *Biomacromolecules*. 2002; 3(2):357–367. [PubMed: 11888323]
10. Wright ER, Conticello VP. *Advanced Drug Delivery Reviews*. 2002; 54(8):1057–1073. [PubMed: 12384307]

11. Wright ER, McMillan RA, Cooper A, Apkarian RP, Conticello VP. *Advanced Functional Materials*. 2002; 12(2):149–154.
12. Szela S, Avtges P, Valluzzi R, Winkler S, Wilson D, Kirschner D, Kaplan DL. *Biomacromolecules*. 2000; 1(4):534–542. [PubMed: 11710178]
13. Winkler S, Wilson D, Kaplan DL. *Biochemistry*. 2000; 39(41):12739–12746. [PubMed: 11027155]
14. Altman GH, Diaz F, Jakuba C, Calabro T, Horan RL, Chen JS, Lu H, Richmond J, Kaplan DL. *Biomaterials*. 2003; 24(3):401–416. [PubMed: 12423595]
15. Rodriguez-Cabello JC, Reguera J, Girotti A, Arias FJ, Alonso M. *Ordered Polymeric Nanostructures at Surfaces*. 2006; 200:119–167.
16. Ferrari, F.; Cappello, J. *Protein-Based Materials*. McGrath, KP.; Kaplan, DL., editors. Birkhäuser; Boston: 1997. p. 37-117.
17. Petka WA, Harden JL, McGrath KP, Wirtz D, Tirrell DA. *Science*. 1998; 281(5375):389–392. [PubMed: 9665877]
18. Cappello J, Crissman JW, Crissman M, Ferrari FA, Textor G, Wallis O, Whitley JR, Zhou X, Burman D, Aukerman L, Stedronsky ER. *Journal of Controlled Release*. 1998; 53(1–3):105–117. [PubMed: 9741918]
19. Dinerman AA, Cappello J, Ghandehari H, Hoag SW. *Journal of Controlled Release*. 2002; 82(2–3):277–287. [PubMed: 12175743]
20. Megeed Z, Cappello J, Ghandehari H. *Pharmaceutical Research*. 2002; 19(7):954–959. [PubMed: 12180547]
21. Qiu WG, Teng WB, Cappello J, Wu XY. *Biomacromolecules*. 2009; 10(3):602–608. [PubMed: 19186950]
22. Lee SJ, Liu J, Oh SH, Soker S, Atala A, Yoo JJ. *Biomaterials*. 2008; 29(19):2891–2898. [PubMed: 18400292]
23. He W, Yong T, Teo WE, Ma ZW, Ramakrishna S. *Tissue Engineering*. 2005; 11(9–10):1574–1588. [PubMed: 16259611]
24. Niklason LE, Abbott W, Gao JM, Klagges B, Hirschi KK, Ulubayram K, Conroy N, Jones R. *Journal of Vascular Surgery*. 2001; 33(3):628–638. [PubMed: 11241137]
25. Khademhosseini A, Langer R, Borenstein J, Vacanti JP. *Proceedings of the National Academy of Sciences of the United States of America*. 2006; 103(8):2480–2487. [PubMed: 16477028]
26. Tsang VL, Bhatia SN. *Tissue Engineering II: Basics of Tissue Engineering and Tissue Applications*. 2007; 103:189–205.
27. Huang ZM, Zhang YZ, Kotaki M, Ramakrishna S. *Composites Science and Technology*. 2003; 63(15):2223–2253.
28. Yoshimoto H, Shin YM, Terai H, Vacanti JP. *Biomaterials*. 2003; 24(12):2077–2082. [PubMed: 12628828]
29. Pham QP, Sharma U, Mikos AG. *Tissue Engineering*. 2006; 12(5):1197–1211. [PubMed: 16771634]
30. Min BM, Lee G, Kim SH, Nam YS, Lee TS, Park WH. *Biomaterials*. 2004; 25(7–8):1289–1297. [PubMed: 14643603]
31. Rho KS, Jeong L, Lee G, Seo BM, Park YJ, Hong SD, Roh S, Cho JJ, Park WH, Min BM. *Biomaterials*. 2006; 27(8):1452–1461. [PubMed: 16143390]
32. Teng WB, Cappello J, Wu XY. *Biomacromolecules*. 2009; 10(11):3028–3036. [PubMed: 19788307]
33. Liu Y, Shao ZZ, Vollrath F. *Chemical Communications*. 2005; 19:2489–2491. [PubMed: 15886780]
34. Vollrath F, Madsen B, Shao ZZ. *Proceedings of the Royal Society of London Series B-Biological Sciences*. 2001; 268(1483):2339–2346.
35. Kato YP, Christiansen DL, Hahn RA, Shieh SJ, Goldstein JD, Silver FH. *Biomaterials*. 1989; 10(1):38–41. [PubMed: 2713432]
36. Zhang YZ, Venugopal J, Huang ZM, Lim CT, Ramakrishna S. *Polymer*. 2006; 47(8):2911–2917.

37. Nagapudi K, Brinkman WT, Leisen J, Thomas BS, Wright ER, Haller C, Wu XY, Apkarian RP, Conticello VP, Chaikof EL. *Macromolecules*. 2005; 38(2):345–354.
38. Yu JH, Fridrikh SV, Rutledge GC. *Polymer*. 2006; 47(13):4789–4797.
39. Yarin AL, Kataphinan W, Reneker DH. *Journal of Applied Physics*. 2005; 98(6):063501.
40. Kim SJ, Jang DH, Park WH, Min BM. *Polymer*. 2010; 51(6):1320–1327.
41. Nagapudi K, Brinkman WT, Leisen JE, Huang L, McMillan RA, Apkarian RP, Conticello VP, Chaikof EL. *Macromolecules*. 2002; 35(5):1730–1737.
42. Buttafoco L, Kolkman NG, Engbers-Buijtenhuijs P, Poot AA, Dijkstra PJ, Vermes I, Feijen J. *Biomaterials*. 2006; 27(5):724–734. [PubMed: 16111744]
43. Taddei P, Monti P. *Biopolymers*. 2005; 78(5):249–258. [PubMed: 15800959]
44. Koenig JL. *Journal of Polymer Science: Macromolecular Review*. 1972; 6(1):59–177.
45. Barth A, Zscherp C. *Quarterly Reviews of Biophysics*. 2002; 35(4):369–430. [PubMed: 12621861]
46. Liivak O, Blye A, Shah N, Jelinski LW. *Macromolecules*. 1998; 31(9):2947–2951.
47. Fung, YC. *Biomechanics: mechanical properties of living tissues*. Vol. 2. Springer-Verlag; New York: 1993. p. 568
48. Gosline J, Lillie M, Carrington E, Guerette P, Ortlepp C, Savage K. *Philosophical Transactions of the Royal Society of London Series B-Biological Sciences*. 2002; 357(1418):121–132.
49. Aaron BB, Gosline JM. *Biopolymers*. 1981; 20(6):1247–1260.
50. McManus MC, Boland ED, Koo HP, Barnes CP, Pawlowski KJ, Wnek GE, Simpson DG, Bowlin GL. *Acta Biomaterialia*. 2006; 2(1):19–28. [PubMed: 16701855]
51. Sell SA, McClure MJ, Garg K, Wolfe PS, Bowlin GL. *Advanced Drug Delivery Reviews*. 2009; 61(12):1007–1019. [PubMed: 19651166]
52. Li M, Mondrinos MJ, Chen X, Gandhi MR, Ko FK, Lelkes PI. *Journal of Biomedical Materials Research Part A*. 2006; 79A(4):963–973. [PubMed: 16948146]
53. Soffer L, Wang XY, Mang XH, Kluge J, Dorfmann L, Kaplan DL, Leisk G. *Journal of Biomaterials Science-Polymer Edition*. 2008; 19(5):653–664. [PubMed: 18419943]
54. Bellingham CM, Lillie MA, Gosline JM, Wright GM, Starcher BC, Bailey AJ, Woodhouse KA, Keeley FW. *Biopolymers*. 2003; 70(4):445–55. [PubMed: 14648756]
55. Zou Y, Zhang YH. *Annals of Biomedical Engineering*. 2009; 37(8):1572–1583. [PubMed: 19484387]
56. Gosline J, Lillie M, Carrington E, Guerette P, Ortlepp C, Savage K. *Philos Trans R Soc Lond B Biol Sci*. 2002; 357(1418):121–32. [PubMed: 11911769]
57. Holzapfel GA, Sommer G, Gasser CT, Regitnig P. *American Journal of Physiology-Heart and Circulatory Physiology*. 2005; 289(5):H2048–H2058. [PubMed: 16006541]
58. Ozolanta I, Teter G, Purinya B, Kasyanov V. *Medical Engineering & Physics*. 1998; 20(7):523–533. [PubMed: 9832028]
59. Sill TJ, von Recum HA. *Biomaterials*. 2008; 29(13):1989–2006. [PubMed: 18281090]
60. Yang L, Van der Werf KO, Fitie CFC, Bennink ML, Dijkstra PJ, Feijen J. *Biophysical Journal*. 2008; 94(6):2204–2211. [PubMed: 18032556]
61. Megeed Z, Cappello J, Ghandehari H. *Advanced Drug Delivery Reviews*. 2002; 54(8):1075–1091. [PubMed: 12384308]
62. Gustafson J, Greish K, Frandsen J, Cappello J, Ghandehari H. *Journal of Controlled Release*. 2009; 140(3):256–261. [PubMed: 19470397]



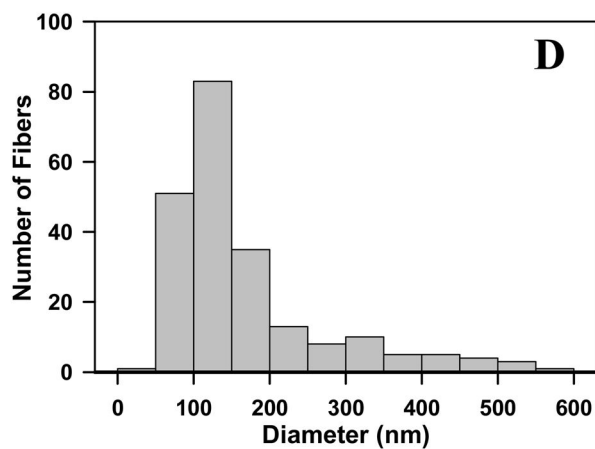
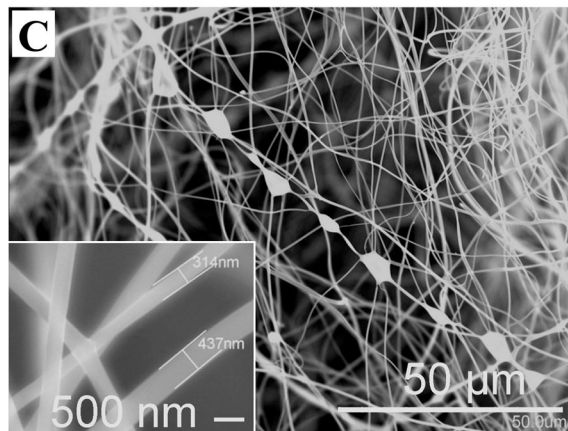
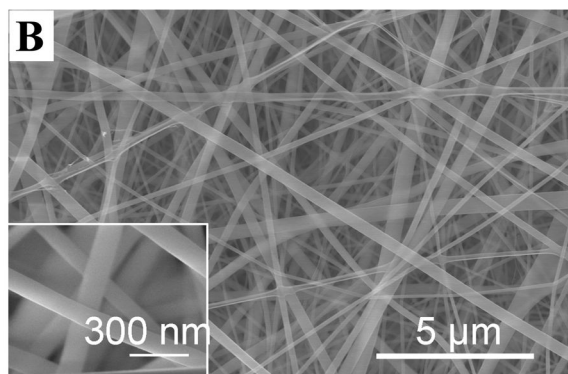


Figure 1. SEM images of SELP-47K nanofibers electrospun from solutions containing protein polymer at concentrations of 50 (A), 150 (B), and 250 mg/mL (C). The diameter distribution (D) of SELP-47K nanofibers shown in (B).

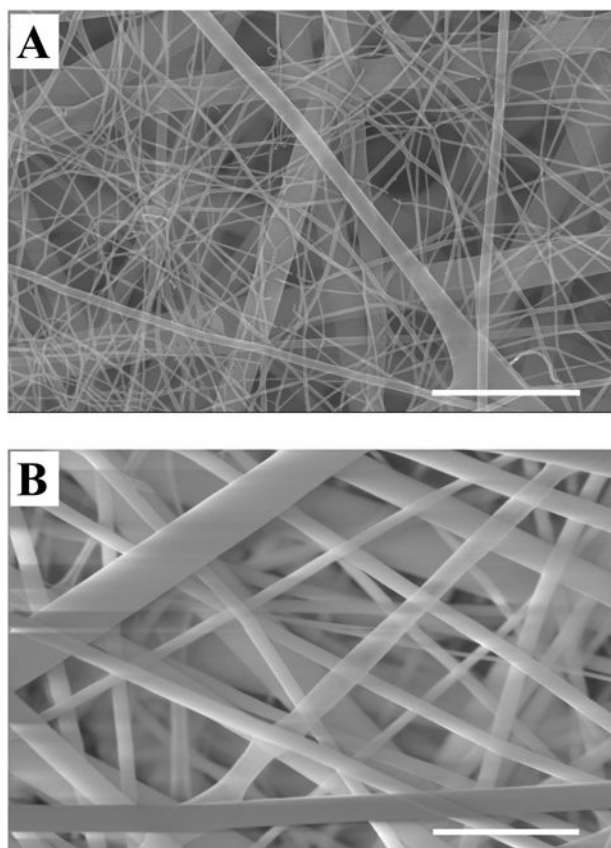


Fig. 2. SEM images of SELP-47K nanofibers from solutions containing protein polymer at concentrations of 150 mg/mL: fibers closer to the glass slide (A) and fibers closer to the needle (B). Scale bars: 1 μ m.

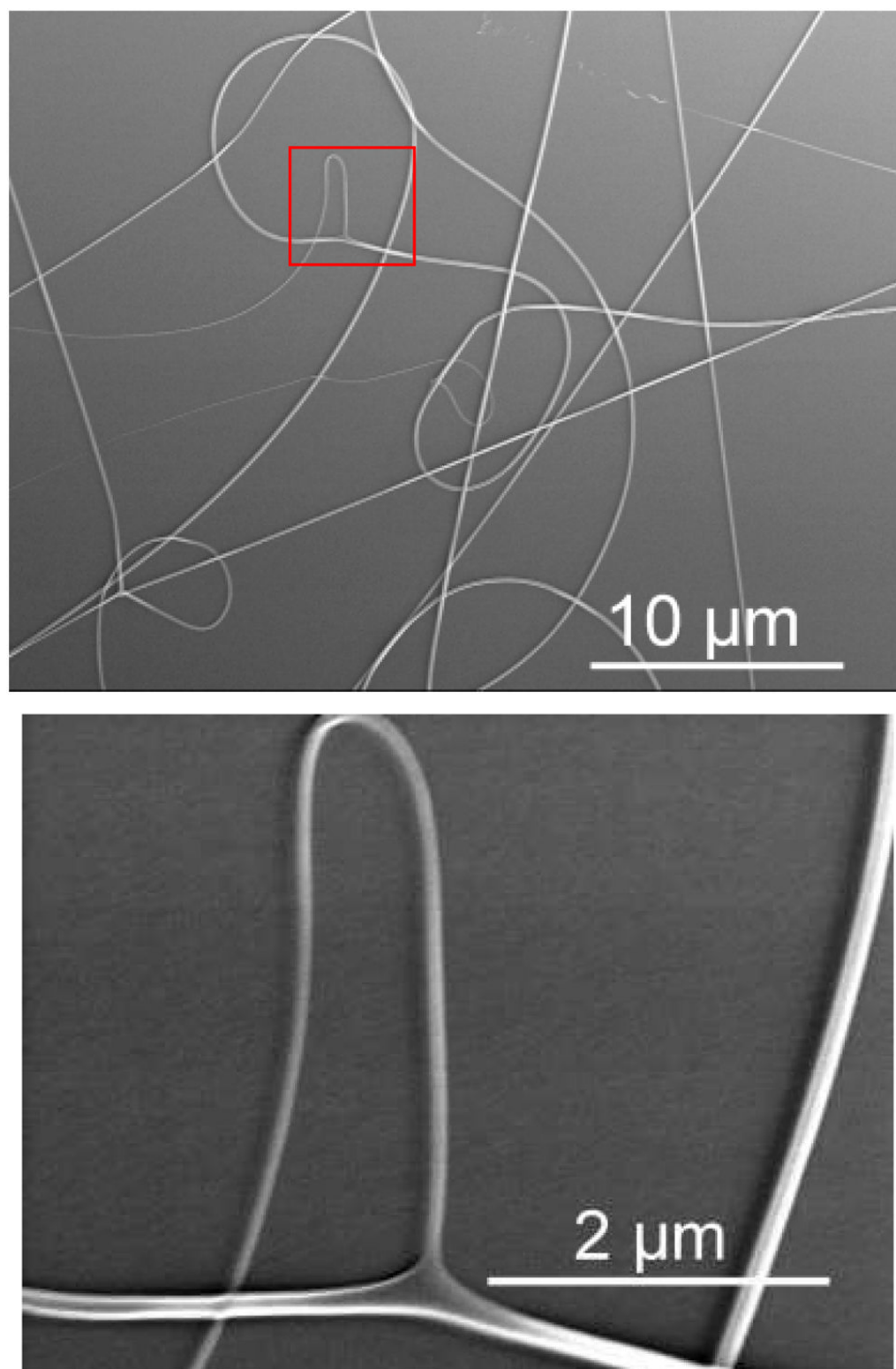
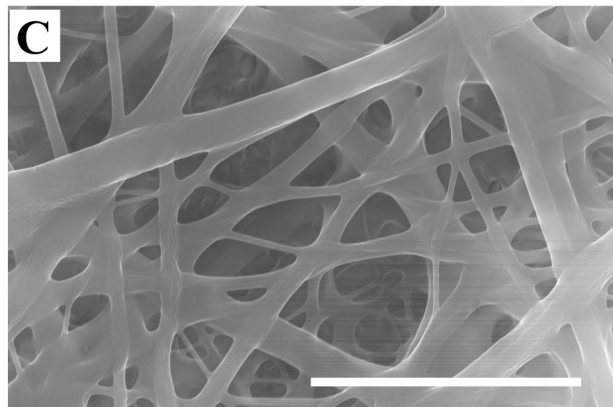
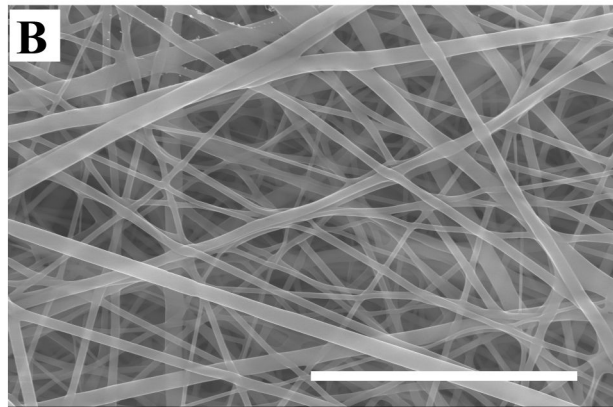
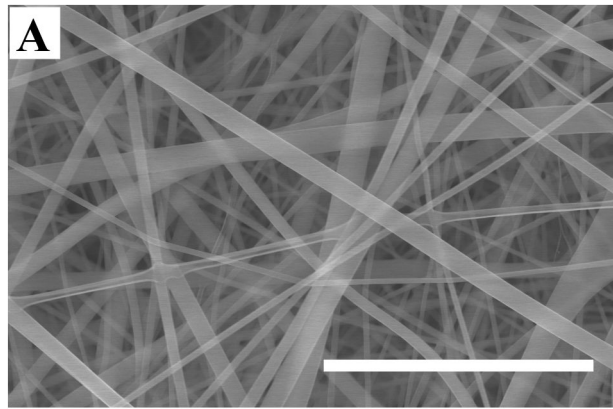


Fig. 3. Fiber branching or bifurcation was examined in the electrospinning of a 150 mg/mL SELP-47K solution in formic acid.



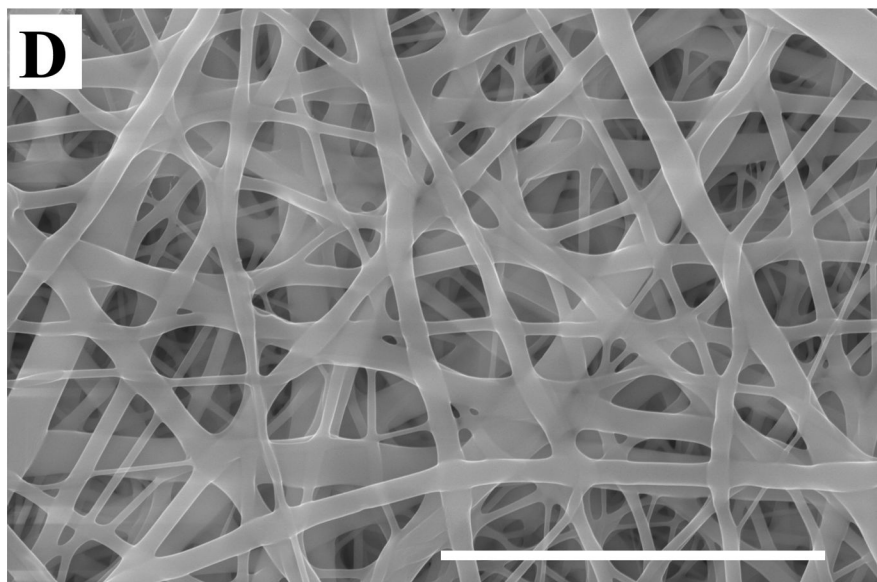


Fig. 4. SEM Images of as-spun (A), MeOH- (B), GTA- (C), and MeOH-GTA-treated (D) SELP-47K fibrous scaffolds electrospun from a 150 mg/mL protein solution. Scale bars: 5 μm .

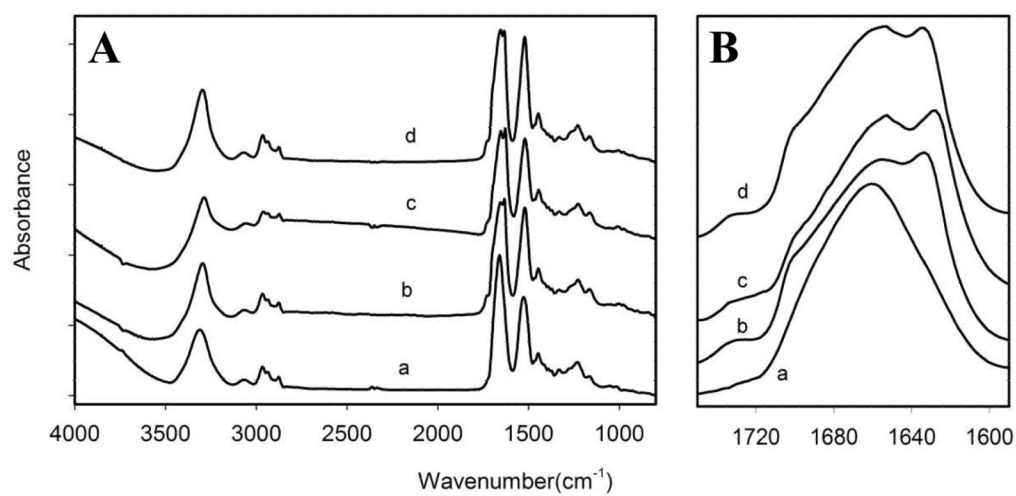


Fig. 5. FTIR spectra of SELP-47K nanofibrous scaffolds in the 800–4000 cm⁻¹ (A) and in the Amide I (B) range: non-treated (a), MeOH-(b), GTA-(c), and MeOH-GTA-treated scaffolds (d). Absorbances were normalized at the amide I band.

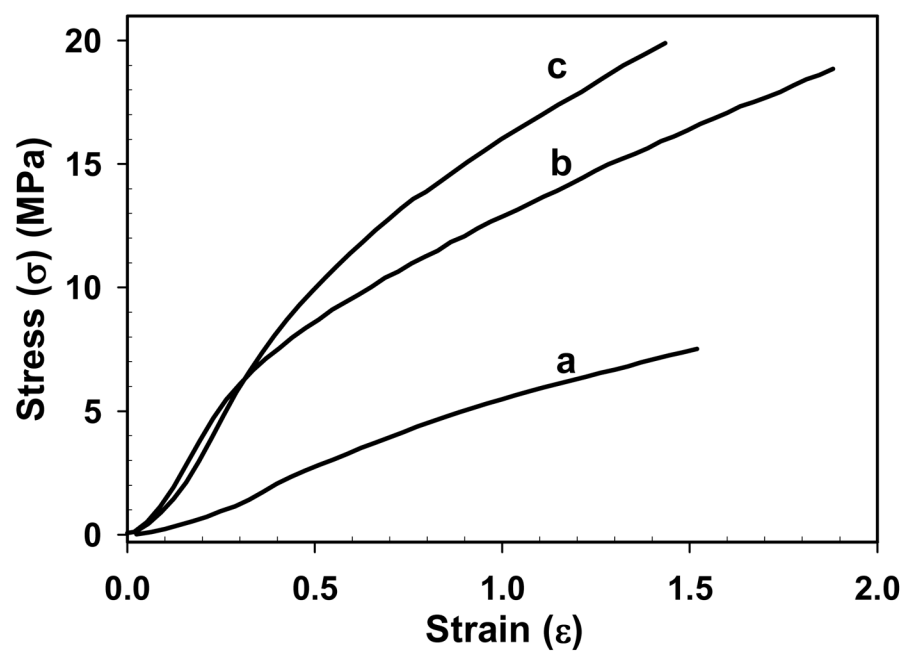


Fig. 6. Representative tensile stress-strain curves of MeOH- (a), GTA- (b), and MeOH-GTA-treated (c) SELP-47K nanofibrous scaffolds.

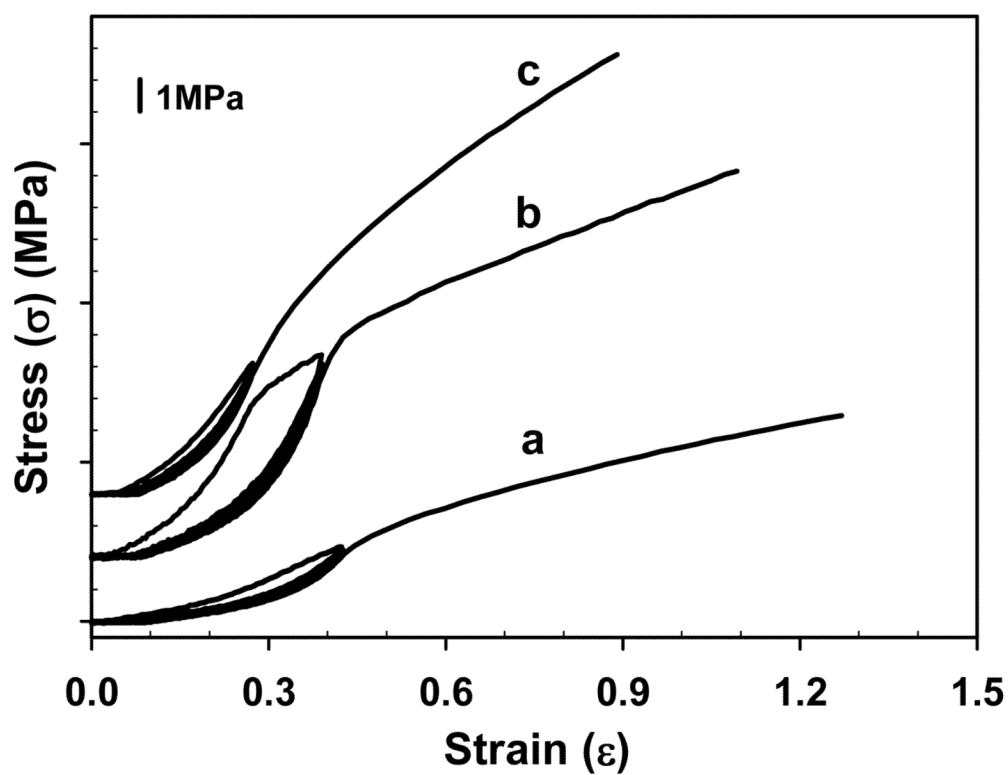


Fig. 7. Representative preconditioning behavior of MeOH- (a), GTA- (b), and MeOH-GTA-treated (c) SELP-47K nanofibrous scaffolds. (Curves were vertically shifted for better clarity.)

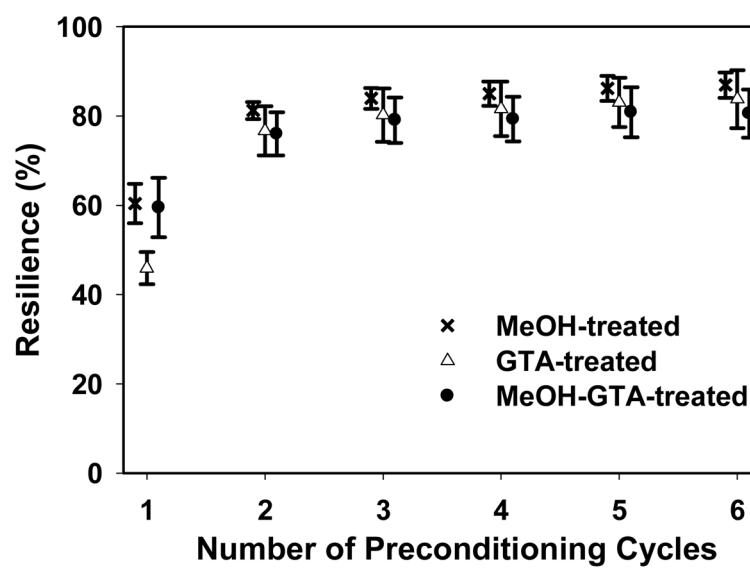


Fig. 8. Resilience of SELP-47K nanofibrous scaffolds as a function of the number of preconditioning cycles. (Curves were horizontally shifted for better clarity.)

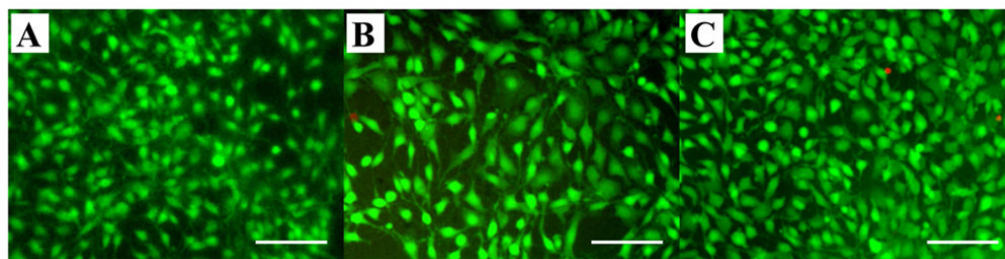


Fig. 9. Fluorescent staining for cell viability of 3T3 fibroblasts grown on MeOH- (A), GTA- (B), and MeOH-GTA-treated (C) electrospun SELP-47K scaffolds for 5 days. Living cells were in green and dead cells were in red. Scale bars: 50 μm .

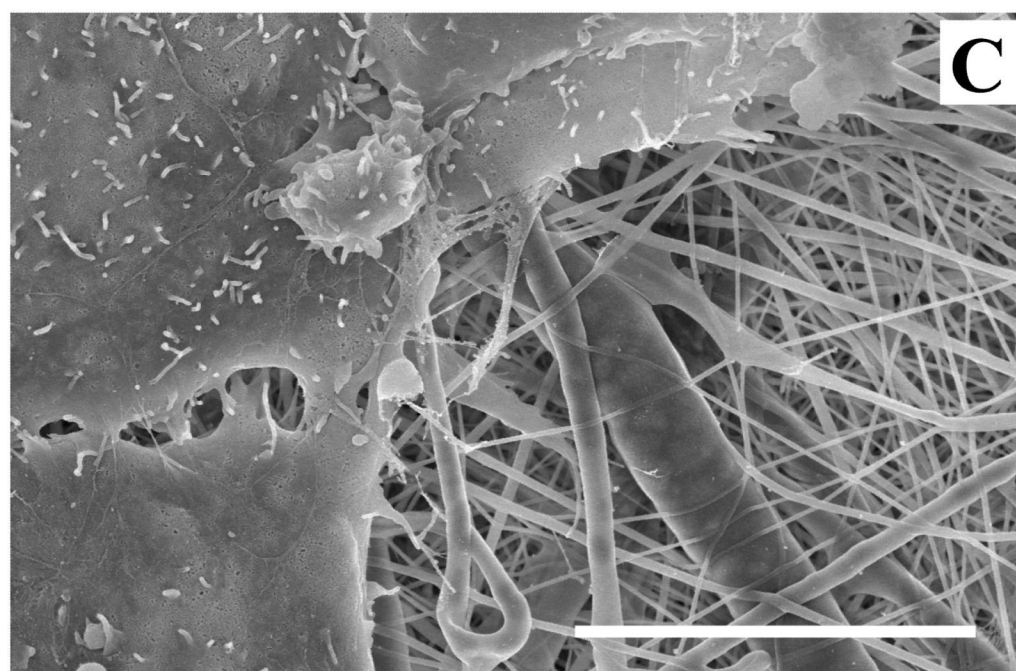
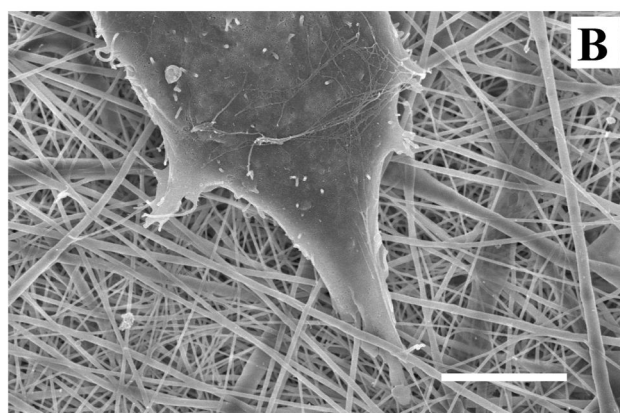
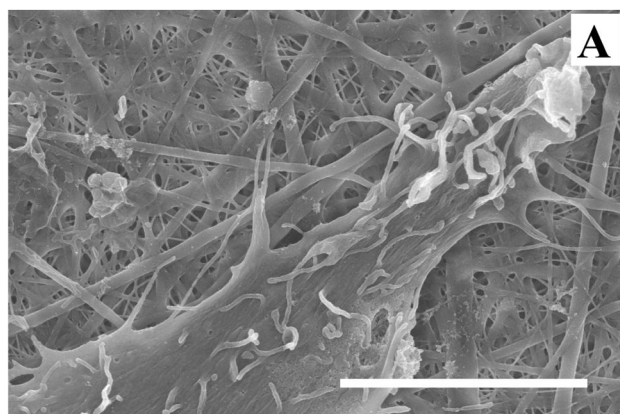


Fig. 10.

SEM images revealed that 3T3 fibroblasts interacted with MeOH- (A) and GTA-treated (B) SELP-47K nanofibrous scaffolds, and with each other (C) on GTA-treated scaffolds. Images were taken 6 days after the initial cell seeding. Scale bars: 10 μm .

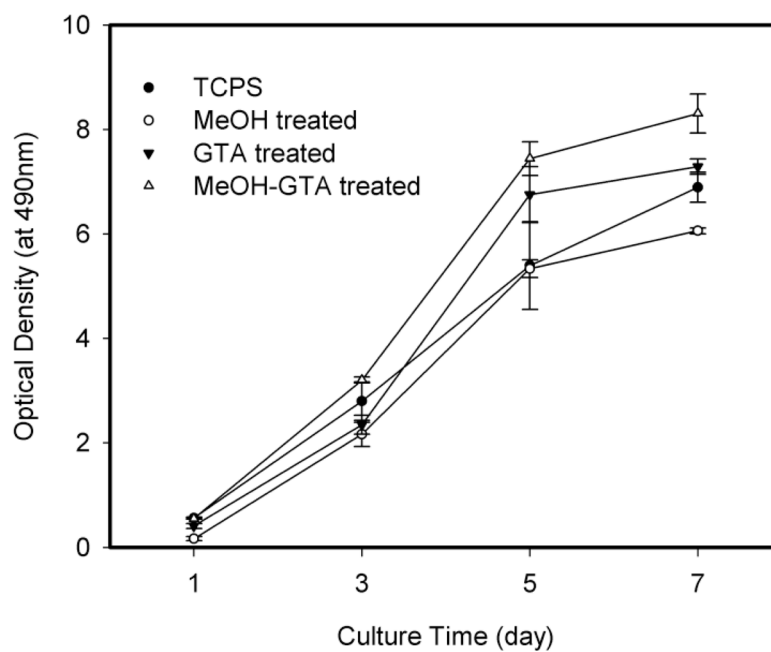


Fig. 11. Proliferation profiles of 3T3 fibroblasts grown on electrospun SELP-47K nanofibrous scaffolds up to 7 days.

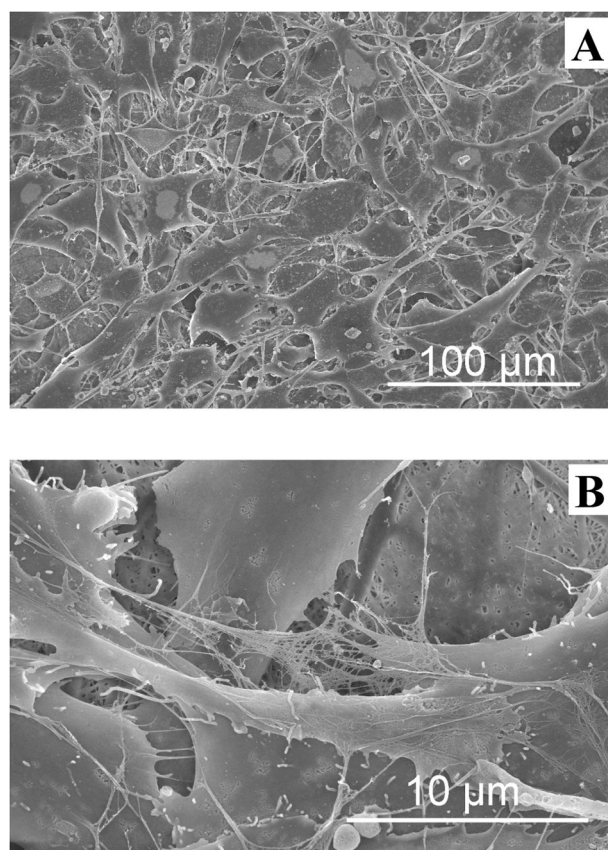


Fig. 12. SEM images showed more than one layer of 3T3 fibroblasts grown on MeOH-GTA-treated (A) and ECM nanofilaments regenerated by cells on GTA-treated scaffolds (B). Images were taken 6 days after the initial cell seeding.

Table 1

Mechanical properties of fully hydrated SELP-47K nanofibrous scaffolds before and after mechanical preconditioning^a

	<i>E</i> (MPa)	σ_T (MPa)	ϵ_F	<i>r</i> (%)
MeOH-treated	3.7±1.2/3.4±0.7	7.2±2.3/5.7±1.4	1.3±0.3/1.1±0.2	60.4±4.4/86.9±2.8
GTA-treated	18.2±3.3/10.6±1.6	14.1±3.8/8.0±3.3	1.3±0.4/0.7±0.2	45.9±3.6/83.8±6.5
MeOH-GTA-treated	13.8±3.7/13.2±4.2	15.8±5.3/13.5±4.4	1.0±0.3/1.1±0.3	59.5±6.7/80.6±5.4

^aValues separated by a slash “/” are the mechanical properties of SELP-47K scaffolds before and after preconditioning, respectively.

Abbreviations: *E*, elastic modulus measured in the first 20% strain region; σ_T , ultimate tensile strength; ϵ_F , strain at failure; *r*, resilience.

Comparison of the elastic properties of protein-based and protein-blended polymeric nanofibrous scaffolds with data of native human artery and vein.^a

Table 2

	Solvent	Treatment	Elastic Properties		
			E (MPa)	σ_T (MPa)	ϵ_F
SELP-47K scaffolds (this study)					
	formic acid	MeOH vapor	3.4±0.7	5.7±1.4	1.1±0.2
		GTA vapor	10.6±1.6	8.0±3.3	0.7±0.2
		MeOH-GTA vapor	13.2±4.2	13.5±4.4	1.1±0.3
type I collagen scaffolds ³¹	HFP	GTA vapor	7.4±1.2		
Fibrinogen scaffolds ⁵⁰	HFP	MeOH	0.19~0.55	0.28~0.60	0.7~1.1
type I collagen blended PDO scaffolds ⁵¹	HFP	no treatment	15.8±3.7	5.9±1.1	0.7±0.1
type III collagen blended PDO scaffolds ⁵¹	HFP	no treatment	22.3±2.9	6.1±0.7	1.5±0.2
gelatin-elastin blended PLGA scaffolds ⁵²	HFP	UV light		12~43 ^b	~0.6 ^b
B. MORI silk blended PEO scaffolds ⁵³	H ₂ O	MeOH	2.45±0.47	2.42±0.48	
porcine aortic elastin (native) ⁵⁴			0.81	1.02	1.03
bovine aortic elastin (native) ⁵⁵			0.1~0.35 ^c		
bovine ligament elastin (native) ⁵⁶			1.1	2.0	1.50
Human coronary artery ^{57,58}			1.1~4.1 ^d	0.4~1.4 ^d	1.6~1.9 ^d
Human femoral artery ⁵¹			9~12	1~2	1.6~1.8
Human saphenous vein ⁵¹			43	3	1.11

^aAll scaffolds were tested in hydrated state.

^bmechanical properties depend on the protein/polymer compositions.

^ctangent modulus in the circumferential direction.

^dmechanical properties depend on patient's age and gender and artery's tissue composition (i.e., adventitia, media, intima) and orientation (i.e., circumferential, longitudinal).

Abbreviations: HFP, 1,1,1,2,2,2-hexafluoro-2-propanol; PDO, polydioxanone; HFP, 1,1,1,3,3,3-Hexafluoro-2-propanol; PLGA, poly(lactide-co-glycolide); UV, ultraviolet; PEO, poly(ethylene oxide); E , elastic modulus measured in the first 20% strain region; σ_T , ultimate tensile strength; ϵ_F , strain at failure; r , resilience.